Two-dimensional spin-$\frac{1}{2}$ Heisenberg antiferromagnet: A quantum Monte Carlo study

Miloje S. Makivić and Hong-Qiang Ding
Department of Physics, California Institute of Technology, Pasadena, California 91125
(Received 3 May 1990)

Spin-$\frac{1}{2}$ nearest-neighbor Heisenberg antiferromagnet on a square lattice is studied via a large-scale quantum Monte Carlo simulation. We developed a fast and efficient multispin coding algorithm on a parallel supercomputer, based on the Suzuki-Trotter transformation. We performed high-statistics simulations on lattices as large as 128×128 spins, in the temperature range from $0.25J$ to $2.5J$. We calculated energy, specific heat, uniform and staggered susceptibility, and staggered correlation function, from which we deduce the correlation length. For temperatures higher than J, the results are in excellent agreement with high-temperature series expansion. At low temperatures the long-wavelength behavior is essentially classical. Our data show that the correlation length and staggered susceptibility are quantitatively well described by the renormalized classical picture at the two-loop level of approximation. From the divergence of correlation length, we deduce the value of quantum-renormalized spin stiffness, $\rho_s/J=0.199(2)$. We give evidence that the correlation function is of Ornstein-Zernike type. By comparing the largest measured correlation lengths with neutron scattering experiments on La_2CuO_4, we deduce the value of effective exchange coupling $J=1450\pm30$ K.

I. INTRODUCTION

The discovery of high-temperature superconductors[1] has brought about a resurgence of interest in two-dimensional (2D) quantum antiferromagnets. There are experimental and theoretical indications that spin dynamics plays a crucial role in the new superconducting mechanism, which is believed to originate from purely electronic degrees of freedom.[2–4] Neutron scattering experiments on the parent compound La_2CuO_4 reveal a rich magnetic structure.[4,5] Over a wide temperature range, copper spins in Cu-O planes exhibit strong two-dimensional antiferromagnetic correlations, but without broken symmetry. As the temperature is lowered through the *three*-dimensional Néel ordering temperature (T_N), weak interlayer coupling drives the system into a unique 3D ordered state.

The simplest theoretical description of the system is provided by the spin-$\frac{1}{2}$ antiferromagnetic Heisenberg model (AFHM), which is the strong coupling limit of the Hubbard model at half-filling:[6]

$$H=J\sum_{\langle ij\rangle}(S_i^xS_j^x+S_i^yS_j^y+S_i^zS_j^z)\ . \tag{1}$$

The summation $\sum_{\langle ij\rangle}$ goes over all the nearest-neighbor pairs on a square lattice and S_i is the spin operator at the ith site. The energy scale is set by the effective exchange coupling J ($J>0$ for an antiferromagnet). In what follows we will also express temperature in units of J and set $k_B=\hbar=1$.

Being one of the oldest models of quantum statistical physics, AFHM has merits of its own, apart from its relevance for high-T_c superconductivity. The highly quantum nature of spin-$\frac{1}{2}$ systems is difficult to capture.[7] Analytical approaches employ different perturbation schemes (e.g., spin wave theory,[8] renormalization group approaches,[9] series expansions,[10] large-N expansions,[11] etc.), variational treatments,[12,13] or exact diagonalizations for small systems.[14]

On the other hand, Monte Carlo methods can provide nonperturbative results for finite systems. If the system size is large enough, quantitatively reliable conclusions can be drawn about the thermodynamic limit. Monte Carlo methods have been successfully applied to study both ground-state[15] and finite-temperature properties of AFHM.[16–18] Recently, we carried out a large-scale Monte Carlo calculation of spin correlations in the low-temperature regime. By comparing directly with neutron scattering experiments we determined the exchange constant to be $J=1450\pm30$ K. The divergence of the correlation length revealed an essentially classical behavior, in accordance with the elegant picture advocated by Chakravarty *et al.*[9] Part of this work has been previously reported in Ref. 19.

The purpose of this paper is twofold: to present details of the computational method (which we believe is a more efficient variation of the previous ones) and to provide additional results, including the behavior of thermodynamic quantities: energy, specific heat, and susceptibilities. The organization of the paper is as follows. In Sec. II we give an outline of the Suzuki-Trotter quantum Monte Carlo method, and explain how it was implemented in our calculation. Section III pertains to the thermodynamics of the system, while Sec. IV deals with spin correlations and staggered susceptibilities. Experimental implications are discussed in Sec. V. Section VI is a summary.

II. THE COMPUTATIONAL METHOD

A. Suzuki-Trotter transformation

The Suzuki-Trotter method[20] is a powerful device for investigating quantum spin systems without frustration.

We begin by breaking the Hamiltonian into four pieces, $H=\sum_{i=1}^{4}H_i$, each containing a commuting subset of nearest-neighbor bonds on a square lattice,[20] as shown in Fig. 1. H_1 contains odd bonds in the x direction, H_2 contains odd bonds in the y direction, H_3 contains even bonds in the x direction, and H_4 contains even bonds in the y direction. Then, to obtain the partition function, we apply Suzuki's generalization of the Trotter formula:

$$Z=\mathrm{Tr}e^{-H/T}=\mathrm{Tr}[(e^{-\Delta\tau H})^m]$$
$$=\mathrm{Tr}\left[\lim_{m\to\infty}\left[\prod_{i=1}^{4}e^{-\Delta\tau H_i}\right]^m\right], \quad (2)$$

where m is an integer (Trotter number) and $\Delta\tau=1/mT$. After $4m$ resolutions of unity are inserted between adjacent exponentials, we obtain

$$Z=\lim_{\Delta\tau\to 0}\sum_{\{C\}}\langle C_1|e^{-\Delta\tau H_1}|C_2\rangle\langle C_2|e^{-\Delta\tau H_2}|C_3\rangle\cdots\langle C_{4m}|e^{-\Delta\tau H_4}|C_1\rangle\ . \quad (3)$$

The intermediate states C_j which are chosen to diagonalize S_z, may be regarded to belong to different time slices. Therefore, the original 2D quantum system of size $L\times L$ is mapped onto the equivalent 3D classical system of size $L\times L\times 4m$. Since the exponential of H_i factorizes into a product of exponentials involving only two spins on a bond, the classical system consists of interacting four-spin plaquettes. The Boltzmann weight, associated with an interacting plaquette configuration is given by the following matrix element:[21]

$$W=\langle S^z_{i,t}S^z_{j,t}|e^{-\Delta\tau S_i\cdot S_j}|S^z_{i,t+1}S^z_{j,t+1}\rangle\ , \quad (4)$$

where i,j correspond to a particular bond, while $t,t+1$ denote two adjacent time slices. Due to conservation of S_z, only 6 out of 16 spin configurations of a four-spin plaquette have nonzero Boltzmann weights.[21] They are listed in the Appendix.

In the early stages of this work we also experimented with another basis set: the coherent spin states.[22] A particular set of coherent spin states can be obtained by applying the spin rotation operator, parametrized by angles θ and ϕ on the unit sphere, to the spin down state: $|\theta\phi\rangle=R(\theta,\phi)|S_z=-\frac{1}{2}\rangle$. The continuous labels θ and ϕ may be regarded as generalized quantum numbers of the ordinary basis sets. The coherent states, though not orthogonal, are overcomplete. Hence, they can provide a valid resolution of unity. Being continuous, it is conceivable that they would be more appropriate to capture the dynamics, which is dominated by spin waves. However, they lead to complex transition probabilities and the phase fluctuations destroy the statistics.

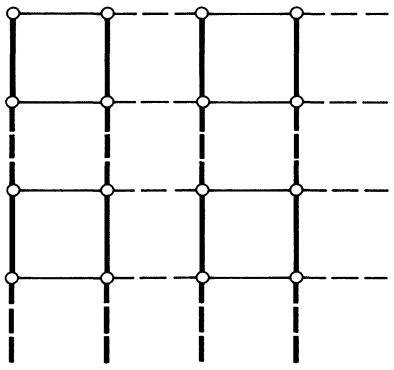

FIG. 1. The breakup of the Hamiltonian: In the x direction, H_1 includes bonds indicated by the solid links; H_3 includes bonds indicated by the broken links. Similarly for H_2,H_4 in the y direction.

B. The updating procedure

The updating procedure has to be ergodic and must not violate the quantum conservation laws. Any allowed update can be achieved as a sequence of updates of pairs of spins on plaquette edges. Since each spin is shared by two plaquettes, it follows immediately that one has to flip a *closed loop of spins*.[21] The conservation of S_z imposes the following constraints. If two spins on a horizontal edge of an interacting plaquette are being updated (both spins on the same time slice), the conservation law requires that the two spins be opposite. If two spins on a vertical edge of an interacting plaquette are involved, one may update the spins only if they are both up or both down.

We generate all possible closed loops under these constraints by exponentiating a set of four types of elementary updates that mimic the generators of the fundamental homotopy group on a torus, with the conservation law built in. The toroidal geometry is the consequence of spatial periodic boundary conditions (to preserve translational invariance) and periodic boundary conditions in the time direction (required by the trace operation).

We have two types of local updates and two types of global updates.[23] The local updates are homotopic to the unit loop. The simpler local update ("space" flip) is shown in Fig. 2. One searches for a noninteracting loop ("space" loop), bounded by the edges of four interacting plaquettes. A "space" loop belongs to a single time slice. Due to the constraint, one may attempt to flip the four spins on a "space" loop [according to the Boltzmann weight in Eq. (4)] only if they are in a Néel configuration, as shown in Fig. 2.

Another local update ("time" flip) is shown in Fig. 3. It involves a noninteracting loop, extending in the time direction ("time" loop), bounded by eight interacting plaquettes. There are eight spins involved in the flip. Again, the flip is attempted only if the spins are in a Néel configuration; i.e., the four spins on one vertical edge are all the same and opposite from the four spins on the oth-

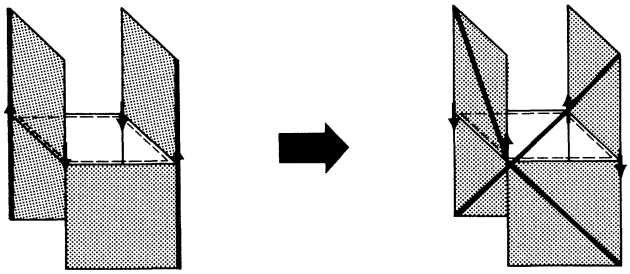

FIG. 2. A "space" flip. The dashed line denotes a noninteracting plaquette lying in spatial dimensions. The four shaded plaquettes extending in the time direction are the interacting ones. After the four spins are flipped, the two world lines (denoted by the heavy solid lines) twist around each other.

er edge, as shown in Fig. 3.

The global update in time direction is shown in Fig. 4. One searches for a straight line of all up or all down spins, and flips them all. This move is responsible for generating fluctuations of the total magnetization. The efficiency of this type of update depends on how many straight lines of up (down) spins are available. Naively, one would expect that it is increasingly difficult to find such lines as temperature is lowered and number of time slices increased. This is not true, however, since the spatial correlation length grows faster than the system width in the "time" direction L_t. Hence, at low temperatures, in the renormalized classical regime,[9] temporal correlation length always saturates around $\xi_t \simeq L_t$. Indeed, we find that the straight lines are abundant enough at all temperatures we used in the simulations. This enabled us to obtain correct results for the uniform susceptibility, which we calculate from magnetization fluctuations generated by these straight line flips.

In Fig. 5(a), the other type of global update, extending in either spatial direction, is shown. Assuming that the

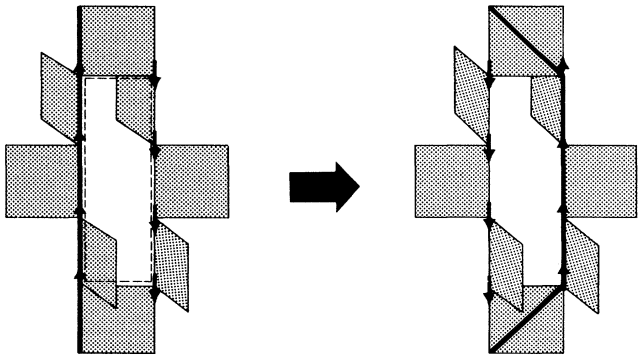

FIG. 3. A "time" flip. The dashed line denotes a noninteracting plaquette. The eight shaded plaquettes surrounding it are the interacting ones. After the eight spins are flipped, the worldline (denoted by the heavy solid line) is distorted. Notice that all plaquettes go in the time direction.

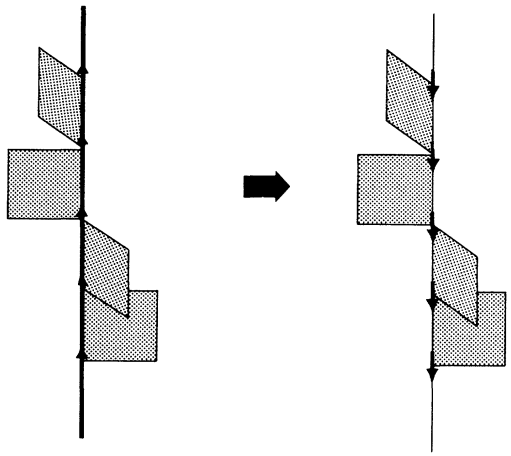

FIG. 4. A "global" flip in the time direction. Only four interacting plaquettes surrounding a straight world line are shown.

numbering of time slices starts from zero, let us choose two adjacent time slices, denoted by t_1 and t_2, such that t_1 is even and t_2 is odd. Consider now a pair of neighboring straight lines, belonging to t_1 and t_2, respectively, such that they run in the y direction, i.e., $x(t_1) = x(t_2) = \text{const}$. It is easy to see that this pair consists of segments that involve only edges of interacting plaquettes. The same is true for a pair $y(t_1) = y(t_2) = \text{const}$, but, in this case, the lower time slice t_1 must be odd and the upper one t_2 must be even. Therefore, global flips in the x and y directions are interleaved. Furthermore, to

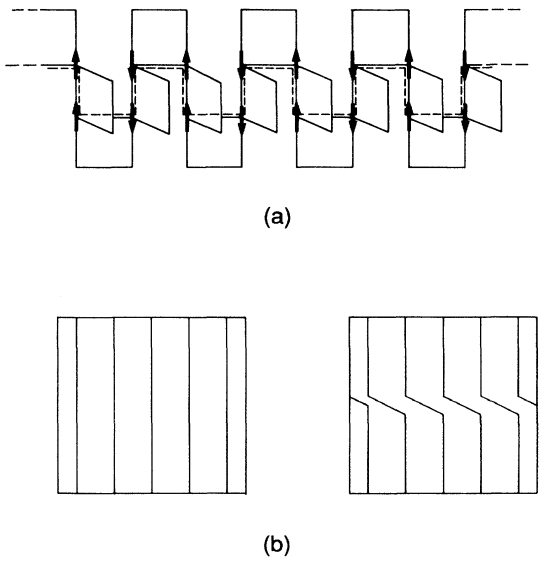

FIG. 5. (a) A "global" flip in spatial directions. The dashed line indicates the string of spins being flipped. The plaquettes shown are all interacting. (b) A configuration with different winding number is reached.

satisfy the conservation law, the two lines must have the same Néel-like spin configurations, as shown in Fig. 5(a).

By employing a well-known connection between spin and boson algebra,[24] this updating procedure can be given a useful alternative interpretation. Let $b_i, b_i^\dagger$ denote ordinary Bose operators on site i. By using a projector $P_i(0)$ onto a state with 0 particles on site i, one defines the operators $a_i = P_i(0) b_i$, $a_i^\dagger = b_i^\dagger P_i(0)$, which vanish outside the subspace with 0 or 1 particle. After the identification $|1\rangle \Longrightarrow |+\rangle$ and $|0\rangle \Longrightarrow |-\rangle$, one has the equivalence $a^\dagger \Longrightarrow \sigma_-$ and $a \Longrightarrow \sigma_+$, where σ_- and σ_+ are spin-lowering and -raising operators. Since $N = a^\dagger a = (1-\sigma^z)/2$, the conservation of S_z may be interpreted as number conservation in this language.

By connecting the sites with spins down (or up, due to particle-hole symmetry), one obtains the world lines of bosons with infinite on-site repulsion (hard core provided by the projector), propagating in imaginary time. There is a unique way of doing this, since the hard core prevents two lines from crossing each other. The updating of the spin system is equivalent to generating all possible configurations of world lines.

The elementary moves have a more transparent interpretation of the boson world-line picture. The "time" flip locally distorts a world line in both spatial directions. Its effect is shown in Fig. 3, and it involves a single world line. The "space" flip involves two nearby world lines, and its effect is to exchange them and wrap them around one another, as shown in Fig. 2. Due to this permutation, the world lines do not necessarily close on themselves, although the spin configuration is periodic in time.

The global move in time direction destroys or creates static particles (holes) (Fig. 4). It connects subspaces with different particle numbers (magnetization). This global move is easily generalized to the world lines of any shape (mobile particles), but the program is much more efficient for straight world lines.

Since the world lines are on a torus they will belong to different homotopy classes, characterized by their winding numbers N_x and N_y. The global move in spatial directions is responsible for connecting these distinct topological subspaces. It breaks and reconstructs a number of world lines of order L, and its effect is shown in Fig. 5(b).

C. Multispin coding and parallel implementation

To achieve a high level of speed and efficiency, we implemented this Suzuki-Trotter method via a multispin coding algorithm. The spins, which are one-bit objects, are packed into 32-bit computer words, along the imaginary time direction. The algorithm is most efficient if the words are completely packed, which means that the number of time slices has to be a multiple of 32 (or, alternatively, the Trotter number m should be a multiple of 8).

All the necessary checks and updates can be implemented through bit-wise logical operations on words. The same principles are applied for both local and global moves, but it is easier to illustrate them for local moves, as shown in Fig. 6.

A pair of adjacent words contains eight "time" loops

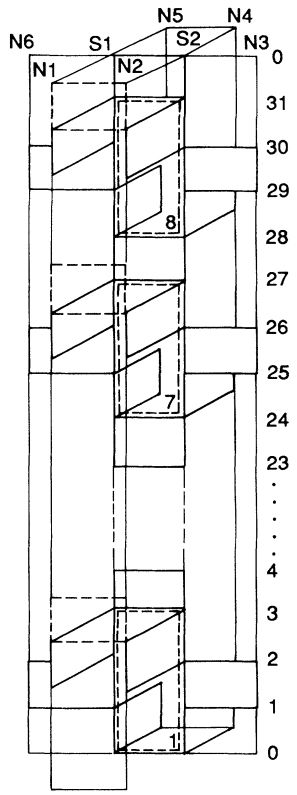

FIG. 6. The vectorized "time" flips are shown. Spins along time direction are packed into computer words. The two 32-bit words $S1$ and $S2$ contain eight "time" plaquettes, indicated by the dashed lines. The plaquettes shown are all interacting ones.

(see Fig. 6). Because every two adjacent "time" loops share an interacting plaquette, we update all four odd "time" loops simultaneously in a vectorized fashion. The other four even "time" loops are updated next. Many of the useful quantities obtained in updating the four odd ones will also be used for the four even ones. We now briefly illustrate the scheme. We want to update the odd "time" loops 1, 3, 5, and 7 of the spin words $S1$ and $S2$ in Fig. 6. We first compute $F = S1$ [XOR], $S2$, and then $W = F$ [AND] MASK1, where MASK1 has 1s located at the proper position of the "time" loop 1 MASK1 $= (0 \cdots 01111)$, [AND] is the conjuctive and [XOR] is the exclusive or Boolean operators. The flip of "time" loop 1 is allowed if W [AND] MASK1 = MASK1 and ($S1$ [AND] MASK1) + ($S2$ [AND] MASK1) = 16 (which means that all four spins in $S1$ must be down and the four spins in $S2$ must be up, or vice versa). $S1$ is also XOR-ed with $N1$, $N6$, and $N5$ to obtain $E1$, $E6$, and $E5$, the information needed to compute the energy due to the three interacting plaquettes on the $S1$ side (see Fig. 3). Similarly, $S2$ is XOR-ed with $N2$, $N3$, and $N4$. Finally, $S1$ or XOR-ed with ($S1$ [right-shift] 1) to obtain C, which contains the information about the upper and lower interacting plaquettes (which are shared by adjacent "time" loops). After masking $N1$–$N6$ and C with appropriate masks, we SHIFT, OR them together, to obtain $X1$ and

$X2$, which contain the information about the eight "time" loops shared by $S1$ and $S2$. Notice that $N1-N6$ are used only *once* for all of the eight "time" loops.

To retrieve the information specific to the "time" loop 1, we calculate $I1=X1$ [AND] MASK1 and $I2=X2$ [AND] MASK1. $(I1,I2)$ is a pair of small integers in one-to-one correspondence with the spin configuration: it uniquely determines the transition probability. Thus $(I1,I2)$ is used as an index to fetch the transition probability stored in a small lookup table calculated at the beginning. Upon acceptance, the proper four spins in $S1$ are flipped by $S1=S1$ [XOR] MASK1, and similarly for $S2$. The update of the "time" loop 3 proceeds in the same manner as for loop 1, after left-shifting MASK1 for 8 bits, and similarly for loops 5 and 7. Once "time" loops 1,3,5,7 are completed, we need to recalculate C only, and the entire process is repeated for even loops. Notice that the only floating-point operation in these updates is a random-number comparison, required for the Metropolis accept/reject test.

Four adjacent words contain eight "space" loops, which can be even more easily vectorized. They can be updated without alternating even and odd ones, since they are decoupled.

The global move in time direction is very easy to implement with this type of spin packing. One has to check whether bits are all either 0's or 1's, then to XOR the word to be flipped with four neighboring words to get the transition probability. The same principles are used to implement the global flip in spatial directions, but the actual procedure is much more complicated. It is desirable to have the simplest possible spin interaction in order to minimize the complexity of the various tests needed to determine the transition probability. For this reason, we believe that a "bond-type" decomposition[20] is preferable due to the simplicity of spin interactions, although the spin packing could be done with any other decomposition, such as "cell-type" breakup, which leads to more complicated eight-spin interactions.[25,23]

The code was adapted for a parallel supercomputer, the 32-node Caltech/JPL MarkIIIfp Hypercube at Caltech.[26] The nearest-neighbor interaction in the system allowed for an efficient parallelization. The hypercube topology of the processor-node system is mapped onto a 2D grid. Then, the processor nodes were configured as disconnected rings, so that several independent systems were running at the same time [see Fig. 7(a)]. Each processor is assigned a piece of the 3D lattice, consisting of a number of (x,t) planes, as shown in Fig. 7(b). The communication between processors is required only if the boundary spins are updated and involves only nearest-neighbor processors.

A good measure of the degree of parallelism in an application is the speedup, defined as $S(M)=t_1/t_M$, where t_M is the time elapsed on a parallel computer with M nodes, while t_1 is the time required for the same application, but on a sequential computer. The concurrent efficiency is defined as speedup per node, $\varepsilon=S(M)/M$, and its maximum theoretical value is 100%. The efficiency of our program is very high (around 90%).[27] In the simulation we used a parallel version of the generalized Fibonacci additive random numbers generator,[28] which has a period longer than 2^{127}.

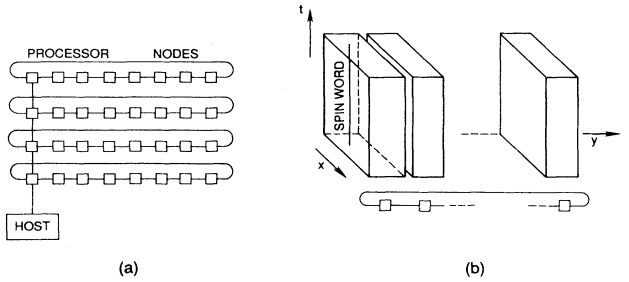

FIG. 7. (a) The configuration of the hypercube nodes. In this example, 32 nodes are configured as 4 independent rings, each consisting of 8 nodes. Each ring runs an independent simulation. (b) The decomposition of the physical space of each lattice among the nodes in a ring.

On a 32-node hypercube, for a $64\times64\times128$ equivalent classical system, the "time"-flip updates are running at an average speed of 1.8×10^6 trials per second. The other local update, the "space" flip, has the average rate of 2.6×10^6 trials per second. The average rate of the global flips in the temporal direction is about 1.7×10^5 trials per second. The computations presented here took about 1000 h of central-processing-unit (CPU) time on a 32-node hypercube (roughly equivalent to about 1200 h on the Cray Research, Inc. X-MP supercomputer).

D. Simulation and measurements

We tested the algorithm on a 4×4 system, where the exact results are available. It is necessary to include *all* types of updates to obtain correct results, since the system is far away from the thermodynamic limit. However, in Table I, we show the results with and without the spatial global moves for a much larger system (32×32). We also plot the correlation functions for the two cases (Fig. 8). It is apparent that this system size is large enough to eliminate any systematic differences.

The equivalence between the quantum system and the classical one is exact only in the limit of infinite m. In practice one works with finite values of m (or, equivalently, $\Delta\tau\neq0$), which is a source of systematic error. The error thus introduced is small and well controlled. It is of order $(\Delta\tau)^2$, and it is volume independent for sufficiently large systems, being proportional to the norm of commutators $[H_i,H_j]$.[29] For a wide class of observables, one may use the extrapolation[20,29]

$$A(m)=A(\infty)+a/(mT)^2+b/(mT)^4+\cdots, \qquad (5)$$

where $A(\infty)$ is the correct value. Commonly, only the leading order term is retained, so one extrapolates linearly in $(1/mT)^2$. A different approach, the one we adopted, is to fix the value of $(1/mT)^2=(\Delta\tau)^2$ to a very small number at every temperature, by choosing appropriate values of m.[30] Our choice of $\Delta\tau\leq0.07$ is small enough to ensure that the systematic error is within the statistical errors of the simulation. To prove this, at $T=0.45$, we used three different values of the Trotter number:

TABLE I. Temperature, Trotter number, linear size, energy, specific heat, uniform susceptibility, correlation length, and exponent λ.

T	m	L	$-E$	Cv	χ	ξ	λ
2.5	16	24	0.1600(2)	0.067(1)	0.201(1)		
2.0	16	24	0.2003(3)	0.102(1)	0.227(2)	0.569(2)	0.5
1.5	16	24	0.2666(6)	0.168(3)	0.256(3)	0.68(3)	0.51(9)
1.2	16	24	0.328(1)	0.248(3)	0.275(1)	0.83(4)	0.47(16)
1.0	16	32	0.3885(8)	0.322(4)	0.281(2)	0.968(2)	0.36(22)
0.85	16	24	0.439(2)	0.393(1)	0.281(2)	1.21(3)	0.42(6)
0.75	24	32	0.4812(9)	0.43(1)	0.274(1)	1.44(2)	0.46(9)
0.60	24	32	0.5498(8)	0.452(5)	0.259(2)	2.20(4)	0.47(3)
0.50	32	32	0.5946(5)	0.425(3)	0.236(2)	3.5(1)	0.51(3)
0.45	16	32	0.6263(2)	0.412(4)	0.219(1)	5.2(2)	0.51(3)
0.45	32	32	0.6208(5)	0.386(5)	0.221(2)	4.6(2)	0.47(5)
0.40	40	64	0.6341(2)	0.353(5)	0.207(2)	6.5(2)	0.47(4)
0.35	24	64	0.6529(1)	0.283(7)	0.191(1)	9.9(4)	0.44(6)
0.35	48	64	0.6507(2)	0.23(1)	0.190(2)	10.1(5)	0.36(5)
0.30	24	96	0.6655(1)	0.21(3)	0.178(1)	18.0(5)	0.38(2)
0.30	48	96	0.6597(7)	0.19(3)	0.182(3)	17.5(5)	0.40(2)
0.27	48	128	0.6642(1)	0.175(3)	0.173(3)	28.0(1.2)	0.39(2)
0.25	48	32	0.6669(1)	0.091(4)	0.155(7)		

$m=16$, $m=24$, and $m=32$. In Table I we show the calculated values of energy, susceptibility, and specific heat for the three cases, and the extrapolated values. The results show a weak m dependence, and the differences between the extrapolated values and those obtained with the largest value of $m=32$ are within the statistical errors. Additional checks are given below.

Simulations were done on (2+1)-dimensional systems as large as $128\times128\times192$ spins, in the temperature range from $T=2.5J$ to $T=0.25J$. During the simulation, we have carefully monitored the thermal relaxation and the autocorrelation lengths. At each T we did several sufficiently long runs. For example, at $T=0.3$,

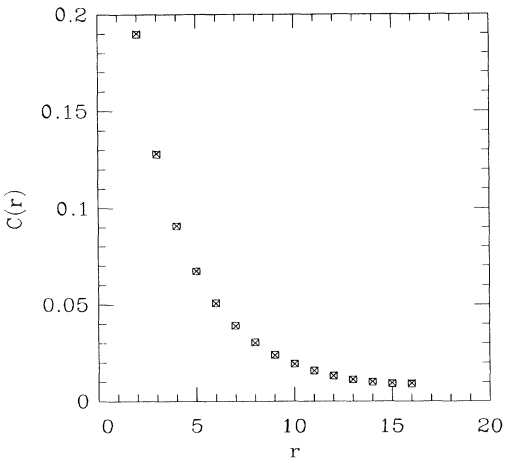

FIG. 8. Correlation functions on the 32×32 lattice at $T=0.45$, $m=24$. Squares denote the run with winding numbers N_x and N_y restricted to 0. Crosses denote the run with nonconstrained winding numbers. The data points clearly overalp. The error bars are of the symbol size.

on the 96×96 lattice, we did $4\times350\,000$ sweeps (four independent runs, 350 000 sweeps each). The thermalization took about 5000 sweeps and the autocorrelation length is about 4000 sweeps. (This all refers to the spin correlation functions for local quantities like energy, both relaxation and autocorrelation times are much shorter.) At higher temperatures and for smaller systems, the runs are slightly shorter. For each of the concurrently running independent systems we calculate the mean and the variance using the correlated sample error analysis. The final result for the measured observable is then obtained by averaging over the independent systems. The variances of independent systems σ_i, $i=1,2,\ldots,N$, are used to calculate the pooled estimator of the common variance, $N\sigma^2=\sum_{i=1}^{i=N}\sigma_i^2$, which yields the quoted error bars.

The global move that changes the magnetization significantly improves the relaxation rate, by about a factor of 3, and its acceptance is quite reasonable (10–50%, depending on T) as explained earlier, contrary to many reports in the literature. In all the simulations, we used this global move. On the other hand, we find that the global move that changes the winding numbers is not efficient and does not improve significantly the relaxation time, so we dropped it in our simulations. Since the quantities we measure do not depend on winding number fluctuations, it follows from standard thermodynamic arguments that this global move may be dropped, and the averages will not be affected in the infinite volume limit.

We calculate energy, specific heat, and uniform susceptibility, as the derivatives of the partition function. They are given by the following averages:[21]

$$E=\left\langle \sum_p F(j_p) \right\rangle , \tag{6}$$

$$CT^2=\left\langle \sum_p \{[F(j_p)]^2-G(j_p)\} \right\rangle -\left\langle \sum_p F(j_p) \right\rangle^2 , \tag{7}$$

$$\chi T=\langle(\Sigma S^z)^2+(\Sigma S^x)^2+(\Sigma S^y)^2\rangle$$
$$=3\langle(\Sigma S^z)^2\rangle\ . \tag{8}$$

The summation goes over all the interacting four-spin plaquettes, labeled by p, and j_p is a label of a particular spin configuration on a plaquette. The functions $F(j_p)$ and $G(j_p)$ represent contributions of individual plaquettes to the total average. The functions F and G, for the allowed four-spin configurations are listed in the Appendix.

More detailed information about the system may be acquired by studying spin correlations. We measured the static staggered spin correlation function

$$C(r)=(-1)^{r_x+r_y}\frac{4}{L^2}\sum_n\langle S_n^z S_{n+r}^z\rangle \tag{9}$$

along the x and y directions [a factor of 4 appears in the definition due to the normalization $C(0)=1$]. This correlation function is a diagonal operator, hence one can choose any time slice for the measurement, make a mask that has a single 1 bit at the location of that time slice, and just XOR the two spin words at positions (n_x,n_y) and (n_x+r_x, n_y+r_y). We used a slightly more complicated procedure. Due to the decomposition, the translational invariance of the Hamiltonian is broken and we want to partially restore it during the measurement. This effect, of course, vanishes in the limit of infinite Trotter number. Since the Hamiltonian is decomposed into four pieces, the spin interactions are periodic in time with period 4, so we calculate the correlation function at four adjacent time slices, corresponding to the lowest four bits in a spin word. All the Trotter numbers in the simulation are larger or equal to 16, thus we have at least two words stacked on top of each 2D lattice site. To improve statistics, we do such a measurement for each word and then average them. Therefore, we do the measurement on a fraction ($\frac{1}{8}$) of the total number of time slices. The correlations are calculated separately along the x and y axes, and then averaged. We check whether they agree within error bars, to ensure that the result is indeed isotropic and as an additional test of thermalization.

Furthermore, we check whether the finite value of the Trotter number will lead to significant systematic effects. At $T=0.45$, we calculated the correlation function using three different values of m, $m=16,24,32$. In Fig. 9 we show these correlation functions. The correlation function has very weak m dependence for such large values of m. We calculated the extrapolated correlation function from these three Trotter numbers using the extrapolation formula of Eq. (5). The extrapolated correlation function and the one with the largest value of $m=32$ are practically indistinguishable. At $T=0.35$ and 0.3 we calculated correlation functions with two different values of $m, m=24$ ($\Delta\tau\simeq 0.14$) and $m=48$ ($\Delta\tau\simeq 0.07$). In Fig. 10 we show the correlation functions at $T=0.35$. Although the width of the time slice is halved, the correlation-function differences are very small. The results at $T=0.3$ are quite similar. The parameters of the fits to these data are given in Table I. The correlation lengths are practically the same. These results show that the

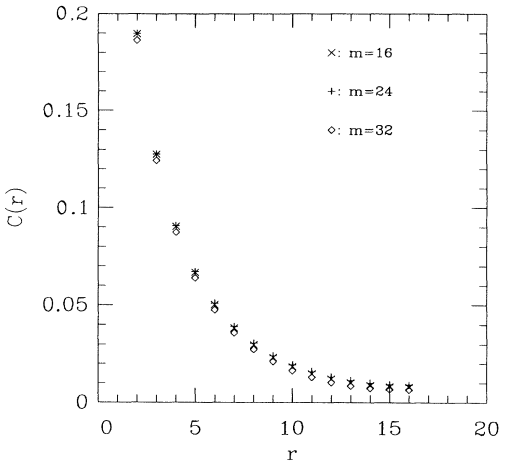

FIG. 9. Correlation functions on the 32×32 lattice at $T=0.45$, with different Trotter numbers m.

values of $\Delta\tau=1/mT$ we are working with are small enough to yield the systematic errors buried within the statistical errors of the simulation and that the extrapolation to $m=\infty$ is unnecessary.

Finally, we calculate the staggered susceptibility,

$$\chi_{\rm st}=\frac{1}{L^2}\left\langle\left[\sum_r(-1)^{r_x+r_y}S_r^x\right]^2\right\rangle\ , \tag{10}$$

following the same approach as outlined for the correlation function. Note that we define the staggered susceptibility to be simply equal to the antiferromagnetic structure factor $C(\pi,\pi)$.

III. THERMODYNAMIC PROPERTIES

A. Energy

The energy as a function of temperature is given in Fig. 11. The size dependence of the energy is negligible. The

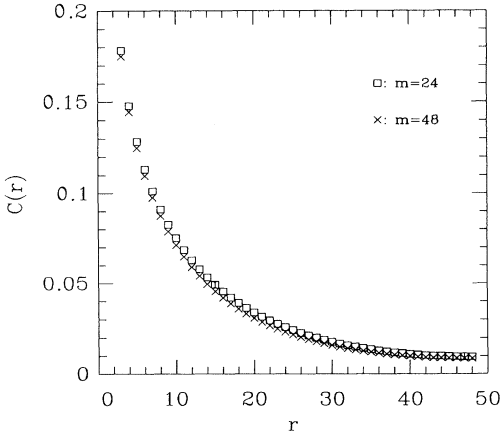

FIG. 10. Correlation functions on the 96×96 lattice at $T=0.35$ with $m=24$ and $m=48$.

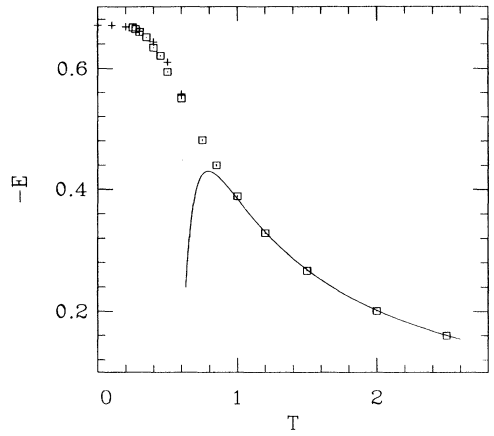

FIG. 11. Energy measured as a function of temperature. Squares are from our work. Pluses are from Ref. 13. The curve is the 10th order high-T expansion (Ref. 30).

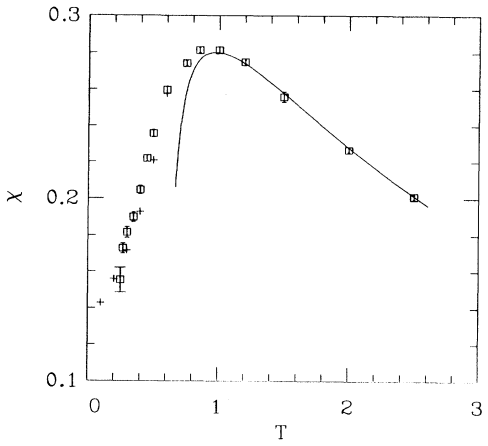

FIG. 12. Uniform susceptibility measured as a function of temperature. Symbols are as in Fig. 11.

results are in good agreement with the calculations performed by other authors on much smaller lattices. The rotational invariance of the Heisenberg Hamiltonian should be preserved by the Monte Carlo simulation. We check this requirement by calculating the energy in two ways: using Eq. (6) and from the nearest-neighbor spin correlation $\langle S_i^z S_j^z \rangle$ assuming full isotropy in spin space. This rotational invariance requirement is satisfied within error bars for all of our data points.

Takahashi developed a modified spin-wave theory, which is expected to be valid in the low-temperature regime, by constructing a variational spin-wave density matrix.[13] The agreement with our calculation is rather good for $T \leq 0.6$. In the high-temperature limit, accurate results can be obtained with high-temperature expansion.[31] We plot our data along with Takahashi's calculation for a 64×64 lattice and high-temperature expansion up to x^{10} ($x = J/T$). Our data smoothly interpolate between these two asymptotic regimes. At $T > 1$, the agreement with the high-temperature expansion is excellent. A note is in order here about the singular-coupling problem.[32] At high T, we used $m = 16$, leading to $mT \simeq 30$. Thus, we are working in the strong-coupling regime, but we do not encounter the "premature convergence" problem, which, in our opinion, may be attributed to insufficient statistics in the earlier simulation.

B. Uniform susceptibility

The data for the uniform susceptibility are presented in Fig. 12. The susceptibility saturates around $T \simeq J$ and then connects smoothly to the high-temperature form.[31] Again, the agreement with high-T expansion is excellent for $T > 1$. For $T \leq 0.6$, we obtain reasonable agreement with Takahashi's result.[13] A major source of the small systematic difference is the incorrect temperature dependence of the variational parameter that determines the spin-wave gap. Note that at $T = 0.35J$ and $0.40J$ the system size is exactly the same as in his calculation, 64×64 spins, so this cannot be attributed to a systematic size dependence. As one goes to higher temperatures, the spin-wave theory fails. The magnetization fluctuations are overestimated, because the ideal density of states overemphasizes the short wavelength spin waves. This is not felt at lower temperatures, since temperature acts as a cutoff.

At temperatures higher than $T = 0.25J$, we attempt to work on system sizes large enough to practically eliminate the finite-size effects. The finite-size effects are expected to get worse at lower temperatures. At $T = 0.25J$, we deliberately simulate a 32×32 lattice, which is 16 times smaller than the lattice used at $T = 0.27J$ (128×128). The sharp drop in the susceptibility is the indicator of a significant finite-size effect for the lattice of this size. This demonstrates that quantitatively reliable results for the zero-temperature limit cannot be obtained by studying relatively small systems (up to 16×16), as was attempted in recent literature.

C. Specific heat

The specific-heat data are shown in Fig. 13. It peaks around $T = 0.6$. The agreement with the high-temperature expansion, in the range $T \geq 1.0$ is excellent. Specific heat is expected to behave as $\propto T^2$, from spin-wave theory, in the low-temperature regime, but we are not going low enough to be able to accurately extract the proportionality constant. Again, we point out that quantitatively accurate results cannot be obtained on small lattices for the $T = 0$ limit. We illustrate this again by plotting the data point for a 32×32 lattice at $T = 0.25$, next to the 128×128 lattice at $T = 0.27$. It is very difficult to obtain accurate results on large lattices in the extreme low-temperature limit due to thermalization problems.

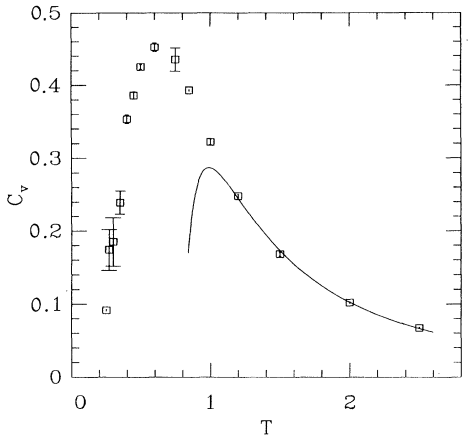

FIG. 13. Specific heat measured as a function of temperature. Symbols are as in Fig. 11.

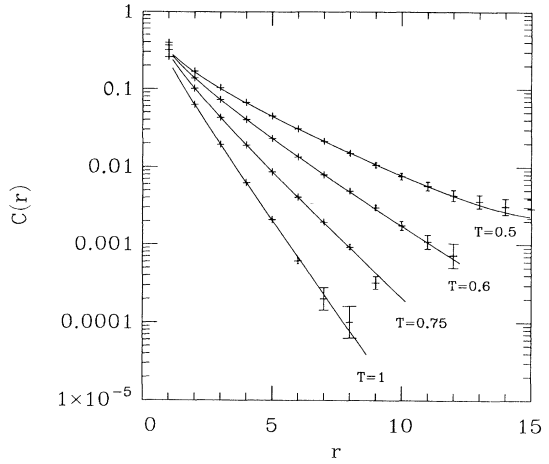

FIG. 14. Correlation functions on the 32×32 lattice at four different temperatures.

IV. SPIN CORRELATIONS

In an infinite system, the correlation function behaves asymptotically as

$$C_\infty(r)\sim Ar^{-\lambda}e^{-r/\xi} \quad \text{as } r\to\infty \ . \tag{11}$$

This expression may be regarded as a definition of the correlation length ξ. In Ornstein-Zernike theory, for a d dimensional system, the exponent λ is equal to $(d-1)/2$. In order to incorporate periodic boundary conditions, for a system of linear size L, we use the following symmetrized form:

$$C_L(r)\sim A[r^{-\lambda}e^{-r/\xi}+(L-r)^{-\lambda}e^{-(L-r)/\xi}] \quad \text{as } r\to\infty \ . \tag{12}$$

The correlation length ξ, the exponent λ, and the amplitude A are treated as fitting parameters. We are not aware of any previous attempt to infer λ for the present model from Monte Carlo data.

We start on a 24×24 lattice at $T=2.5$, where the correlation length is less than a lattice spacing. As the temperature is lowered, we increase the lattice size up to 128×128, to keep $L\geq5\xi$, so that the finite-size effects are very small. The correlation functions at several temperatures are plotted in Fig. 14, along with the best fits. The results of the best fits for ξ and λ are summarized in Table I.

The shortest-range correlations were not included in the fit, since they cannot be described by the asymptotic form of Eq. (11). For larger correlation lengths, usually four or five shortest-range correlations were excluded, while for shorter correlation lengths we discard one or two points. Also, a few points close to half-system size were discarded as the least reliable ones. After these points are discarded, the fits are excellent and are very stable for both long- and short-range cutoffs.

Since the measured values of the exponent λ are very close to $(d-1)/2=\frac{1}{2}$, we conjecture that the correlation functions are of Ornstein-Zernike (OZ) type, as expected on general grounds. This indicates that the puzzling result $\lambda=1$ (as in 3D), suggested by Schwinger boson mean-field theory[11] and modified spin-wave theory,[13] may be an artifact of the approximations involved.

For temperatures less than $T\simeq0.35$, λ drops slightly below $\frac{1}{2}$. This is not unexpected, since the OZ behavior is found only asymptotically, for $r/\xi\gg1$. This condition is no longer true for our data points, as T is lowered ξ becomes large and $r_{\max}\simeq2\xi$. The surprisingly good fit to Eq. (12) shows that an effective value of λ can accommodate these not-so-distant points. This gradual decrease of effective λ is, of course, consistent with $\eta=0$ in an ordered ground state. In previous calculations,[17,18] the correlation functions were described by pure exponentials. Our approach allows for a more consistent comparison with experiment, since the correlation lengths in neutron scattering experiments[4] were obtained by fitting the structure factor data to Lorentzians.

The correlation length as a function of inverse temperature is shown in Fig. 15. The data points fall onto a straight line throughout a wide temperature range. This naturally leads to the exponential fitting form

$$\xi(T)=Ae^{2\pi\rho_s/T} \ . \tag{13}$$

Similar behavior is found in the classical Heisenberg model in 2D (Ref. 33) and is typical for systems at lower critical dimensionality. The fit is indeed very good (χ^2 per degree of freedom is 0.62). The parameters of the fit are listed below [see Eq. (14)].

It was argued by Chakravarty, Halperin, and Nelson[9] (CHN) that, in the parameter regime where the ground state is ordered, the hydrodynamic description is provided by the nonlinear σ model, which has the correct symmetry and excitation spectrum. A perturbative renormalization-group calculation carried out in this model leads to a classical picture, but with the parameters renormalized by quantum fluctuations. Essentially the same result is obtained by Arovas and Auerbach[11] within the framework of a large N expansion, but the

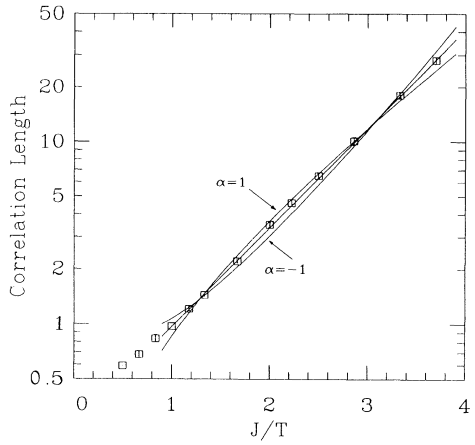

FIG. 15. Correlation length measured at various temperatures. The straight line is fit to Eq. (15). The other curves are the fits corresponding to $A=T^{\alpha}$, $\alpha=1$ and -1. The $\alpha=0.03$ upper bound curve is also plotted, but is indistinguishable from the straight line.

connection with the classical model is not so transparent. Takahashi's variational spin wave theory also turns out to be equivalent to the one-loop result of Ref. 9. However, we show later that the one-loop result is *not* quantitatively correct.

Our calculation is in very good agreement with the renormalized classical picture. Besides verifying the qualitative picture, we provide quantitative results.

In particular, we find that the long-wavelength spin stiffness ρ_s is significantly reduced due to quantum effects, which leads to a much slower growth of the correlation length when compared to the classical case. This renormalization of spin stiffness for a quantum spin S is most conveniently expressed in terms of the renormalization factor $Z_{\xi}^{(S)}$, defined by $\rho_s = JS(S+1)Z_{\xi}^{(S)}$.

The spin stiffness governs the leading exponential divergence, but its value can be accurately calculated only if the leading temperature behavior of the pre-exponential factor $A(T)$ is known. In analytic calculations, $A(T)$ depends on the level of approximation. For instance, in the classical 2D $NL\sigma M$, at the one-loop level this prefactor is temperature independent, $A(T) \propto$ const, while at the two-loop level $A(T) \propto T$.

In a numerical simulation, the extraction of correct temperature dependence is computationally very demanding, since it requires spanning a wide range of correlation lengths and high statistical quality of data. For this reason, our calculation is the first one that can clearly identify the functional *form* of the correlation length from the numerical data. Since the correlation lengths we measure range from 1 to 28, with statistical uncertainties always smaller than 5%, we can easily distinguish between different powers of T in front of the exponential. Our data show that the pre-exponential factor has to be a constant. This follows from a very good quality of the fit given in Eq. (13). The parameters of the fit are

$$\begin{aligned} A &= 0.276(6)\ , \\ \rho_s &= [0.199(2)]J \quad [Z_{\xi}=0.265(2)]\ . \end{aligned} \tag{14}$$

These considerations are illustrated in Fig. 15, where we show our data, along with the best fits obtained with different powers T^{α}, $\alpha=-1,0,1$. Clearly, only the constant prefactor renders a good description of the data. We also fit the data with a general form

$$\xi = AT^{\alpha}e^{2\pi\rho_s/T}\ , \tag{15}$$

regarding α as an additional free parameter. From such a fit, we obtain $\alpha \simeq 0.03$, which may be regarded as an estimate of the upper bound on this exponent. This fit is also shown in Fig. 15, although it is completely indistinguishable from the straight line.

This is in complete agreement with the calculation of CHN, where the classical two-loop term and $1/T$ factor coming from quantum to thermal crossover conspire to give a consant prefactor. The excellent fit to Eq. (13) up to $T \simeq 1.0$ indicates that the renormalized classical region is quite wide. This classical picture remains valid up to a crossover temperature where the Josephson and thermal length scales become compatible.[9] This implies that $2\pi\rho_s \simeq T_{\rm cr}$; i.e., Eq. (13) should be valid while the exponent is of order 1 or less.

Let us compare the renormalized spin stiffness we obtained to those obtained in previous Monte Carlo simulations[17,18] on much smaller lattices ($\leq 20\times 20$). Manousakis and Salvador[17] gave $\rho_s \simeq 0.22$. Gomez-Santos, Joannopoulos, and Negele[18] obtained $\rho_s \simeq 0.159$. At lower temperatures, the former will overestimate the growth of the correlation length, while the latter will underestimate it.

Singh and Huse[10] estimated the spin stiffness constant by expanding around the Ising limit. They obtain $\rho_s \simeq 0.18(1)$, in reasonable agreement with our calculation. Auerbach and Arovas[11] obtained $\rho_s \simeq 0.185$ ($Z_{\xi} \simeq 0.246$), quite close to our result. This is a little surprising considering the mean-field nature of their theory. It is interesting that our calculation gives a *higher* value than the mean-field theory, implicating that the inclusion of fluctuations of all orders in $1/N$ in these SU(N) generalizations of the Heisenberg model actually increases the spin stiffness.

The results for the staggered susceptibility are plotted in Fig. 16. The Ornstein-Zernike form of the staggered spin correlation function implies that $\chi_{\rm st}(T) \propto b(T)\xi^2$. The function $b(T)$ is known to behave as $b(T) \propto T^2$ in the classical 2D $NL\sigma M$ at low temperatures.[34] Our data show that this scaling form applies to the quantum Heisenberg model as well. We plot the staggered susceptibility as a function of $T^2\xi^2$. The data points are reasonably well described by the scaling form $\chi_{\rm st} \propto aT^2\xi^2$. The constant of proportionality a is around 1.65, and can be related to various quantum renormalization factors.[9]

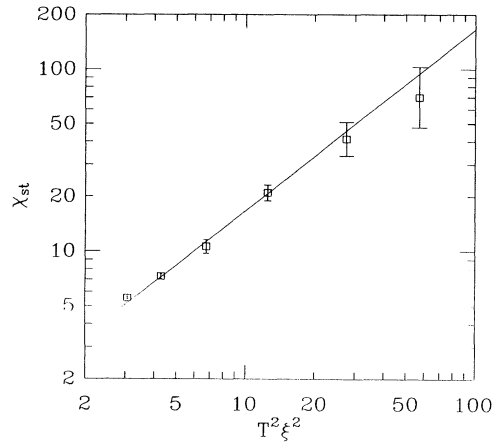

FIG. 16. The scaling plot of the staggered susceptibility. The solid-line fit corresponds to the $NL\sigma M$ result, $\chi_{st} \simeq aT^2\xi^2$, with $a = 1.65$.

V. COMPARISON WITH EXPERIMENTS

It is believed that the Heisenberg model can provide a good description of the undoped high-T_c materials in the insulating phase. We investigate this by comparing the correlation lengths from our calculation with those obtained in neutron scattering experiments.[4]

The effective exchange coupling J and the lattice spacing a are the free parameters in our calculation. Although the Hamiltonian of Eq. (1) is an effective model, the most straightforward approach is to identify the microscopic length scale a with the distance between copper atoms on Cu-O planes (neglecting the orthorhombic distortion): $a = a_H = 3.79$ Å. The only unknown parameter

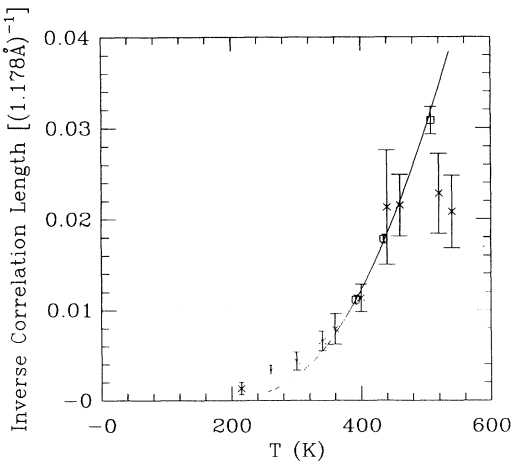

FIG. 17. Inverse correlation lengths of La_2O_4 measured in neutron scattering experiments (Ref. 4), denoted by crosses, and those measured in our simulation, denoted by squares [in units of (1.178 Å)$^{-1}$], $J = 1450$ K. At $T \approx 500$ K, La_2CuO_4 undergoes a structural transition. The curve is the fitting form of Eq. (16).

remains the exchange coupling J, which is to be determined. Choosing $J = 1450$ K, we plot our data points, the best fit [Eqs. (13) and (14)], and the data from neutron scattering experiments[4] in Fig. 17. The agreement is excellent, since our data points are nested between the experimental points. This is a strong indication that the magnetic behavior is indeed dominated by the nearest-neighbor Heisenberg Hamiltonian. Thus, we provide, by a direct comparison with experiment, an independent determination of the exchange constant J:

$$J = 1450 \pm 30 \text{ K} .$$

The uncertainty of ±30 K is estimated by plotting our data points for various values of J, until the deviation from the experimental data points becomes noticeable. This value of J is in very good agreement with the one derived from the spin pair Raman spectrum, by Singh *et al.*:[35] $J = 1480 \pm 70$ K. The agreement between estimates derived from both short- and long-wavelength physics is another indication that the Heisenberg model captures the essential physics. Also, the measurements of spin-wave velocity[5] on a different sample, combined with the quantum renormalization factor for spin-wave velocity,[10] yield a slightly higher estimate, $J \simeq 1550$ K.

The fitting form of Eqs. (13) and (14), with the value

$$\xi(T) = 0.276 a_H e^{1.25 \times 1450/T[\text{K}]} \text{ Å} \tag{16}$$

of J can reproduce some of the experimental data at lower temperatures, which are not accessible to direct simulation. Our choice of J yields a very good agreement with experiment over a wide temperature range and achieves the best agreement between our *data points* and experimental data points. Note, however, that as the 3D Néel temperature is approached, the theoretical curve gives systematically larger correlation lengths than experiment, due to a multitude of small effects, which are not taken care of by the pure Heisenberg Hamiltonian. The very existence of a finite T_N is a manifestation of small symmetry breaking perturbations and interlayer coupling, because the pure Heisenberg model does not have a finite transition, as our simulation demonstrates.

The correlation lengths are very sensitive to the value of spin stiffness, due to the exponential dependence. However, if an error is made in the calculation of ρ_s in units of J, it is possible to adjust the amplitude A and the exchange J, and still obtain reasonable agreement with experimental data. Because of that, the values of J that were used in the literature to fit the experimental data vary from 900 to 1600 K. We believe that our calculation provides an accurate determination of J, in the sense that it is the optimal value, as long as one is satisfied with the description of the real system via the single-coupling model. It is a first principles calculation on the model, with all possible sources of error under control. Our estimate is derived from the data of very high statistical quality, and is based on a direct comparison with experiment. Furthermore, our values of ρ_s [Eq. (14)] and J [Eq. (15)] are in very good agreement with two *independent* series estimates of ρ_s (Ref. 10) and (Ref. 35).

VI. CONCLUSION

The behavior of the 2D quantum Heisenberg antiferromagnet over a wide range of temperatures is investigated via a large-scale quantum Monte Carlo simulation. We developed an efficient multispin coding algorithm on a parallel supercomputer, based on the Suzuki-Trotter transformation. The system sizes are almost 2 orders of magnitude larger than those that were previously achieved. We presented results of high statistical quality for standard thermodynamic quantities like energy, specific heat, and susceptibilities, and compared them with analytical results in appropriate asymptotic regimes. The staggered susceptibility is found to obey the scaling form of the 2D classical $NL\sigma M$.

By studying the spin correlations, we showed that the quantum Heisenberg antiferromagnet with nearest-neighbor exchange coupling behaves very similarly to its classical counterpart, as suggested by the renormalized classical picture of CHN. We have recently performed a similar analysis of the 2D quantum XY model, where we established the presence of Kosterlitz-Thouless phase transition.[36] In other words, these nonfrustrated quantum models are in the same universality classes as their classical analogs.

We show evidence that the correlation functions are of Ornstein-Zernike type. We accurately determine the functional form of the divergence of the correlation length and the renormalization effects due to quantum fluctuations. By comparing the calculated correlation lengths directly with those obtained in neutron scattering experiments, we give an accurate estimate of the exchange coupling, and show that spin correlations in the insulating phase of La_2CuO_4, not too close to the 3D ordering temperature, can be well described by the Heisenberg model.

Our results also provide quantitative assessments of various approximate methods,[9–13] which may be useful for their further improvements.

ACKNOWLEDGMENTS

We are indebted to Michael Cross and Peter Weichman for numerous valuable discussions and to Geoffrey Fox for encouragement and support. This work was supported by U.S. Department of Energy (DOE) Contract No. (DE-GF03-85ER25009 and National Science Foundation (NSF) Grant No. DMR-87-15474. One of us (M.S.M.) thanks the Shell Foundation for partial support.

APPENDIX

To obtain positive matrix elements, it is necessary to perform a canonical transformation on one of the sublattices, say B:[37]

$$H=>UHU^{\dagger}=H=J\sum_{\langle ij\rangle}(-S_i^xS_j^x-S_i^yS_j^y+2S_i^zS_j^z)\ , \tag{A1}$$

where the unitary operator $U=\exp(i\pi\sum_{i\in B}S_i^z)$ maps $S^x=>-S^x$ and $S^y=>-S^y$. There are six nonvanishing matrix elements and six corresponding allowed spin configurations for an interacting four-spin plaquette:

$$\begin{aligned}
W_{++,++}&=e^{-\beta E(1)}\ ,\\
W_{--,--}&=e^{-\beta E(2)}\ ,\\
W_{+-,+-}&=e^{-\beta E(3)}\ ,\\
W_{-+,-+}&=e^{-\beta E(4)}\ ,\\
W_{+-,-+}&=e^{-\beta E(5)}\ ,\\
W_{-+,+-}&=e^{-\beta E(6)}\ ,
\end{aligned} \tag{A2}$$

where $\beta\equiv(k_BT)^{-1}$,

$$\begin{aligned}
E(1)&=E(2)=K=\frac{1}{4m}k_BT\ ,\\
E(3)&=E(4)=-K+\ln[\cosh(2K)]\ ,\\
E(5)&=E(6)=-K+\ln[\sinh(2K)].
\end{aligned} \tag{A3}$$

The functions F and G associated with an interacting plaquette are given by

$$\begin{aligned}
F(j)&=\frac{\partial[\beta E(j)]}{\partial\beta}\ ,\\
F(1)&=F(2)=K/\beta\ ,\\
F(3)&=F(4)=\frac{1}{\beta}\{-K-\ln[\cosh(2K)]\}\ ,\\
F(5)&=F(6)=\frac{1}{\beta}\{-K-\ln[\sinh(2K)]\}\ ,
\end{aligned} \tag{A4}$$

$$\begin{aligned}
G(j)&=\frac{\partial F(j)}{\partial\beta}\ ,\\
G(1)&=G(2)=0\ ,\\
G(3)&=G(4)=\frac{2K}{\beta}\mathrm{sech}(2K)\ ,\\
G(5)(&=G(6)=\frac{2K}{\beta}\mathrm{csch}(2K)\ .
\end{aligned} \tag{A5}$$

[1] J. G. Bendorz and J. A. Müller, Z. Phys. B **64**, 189 (1986); M. K. Wu, J. R. Ashburn, C. J. Torng, P. H. Hor, R. L. Meng, L. Gao, Z. J. Huang, Y. Q. Wang, and C. W. Chu, Phys. Rev. Lett. **58**, 908 (1987).

[2] P. W. Anderson, Science **235**, 1196 (1987); T. M. Rice, Z. Phys. B **67**, 141 (1987), and references therein.

[3] G. Shirane, Y. Endoh, R. J. Birgeneau, M. A. Kastner, Y. Hidaka, M. Oda, M. Suzuki, and T. Murakami, Phys. Rev. Lett. **59**, 1613 (1987); D. Vaknin, S. K. Sinha, D. E. Moncton, D. C. Johnston, J. M. Newsam, C. R. Safinya, and H. E. King, Jr., *ibid.* **58**, 2802 (1987); K. B. Lyons, P. A. Fluery, J. P. Remeika, A. S. Cooper, and T. J. Negran, Phys. Rev. B **37**, 2353 (1988).

[4] Y. Endoh, K. Yamada, R. J. Birgenau, D. R. Gabbe, H. P. Jenssen, M. A. Kastner, C. J. Peters, P. J. Picone, T. R. Thurston, J. M. Tranquada, G. Shirane, Y. Hidaka, M. Oda,

Y. Enomoto, M. Suzuki, and T. Murakami, Phys. Rev. B **37**, 7443 (1988).
[5]G. Aeppli, S. M. Hayden, H. A. Mook, Z. Fisk, S.-W. Cheong, D. Rytz, J. P. Remeika, G. P. Espinosa, and A. S. Cooper, Phys. Rev. Lett. **62**, 2052 (1989).
[6]J. E. Hirsch, Phys. Rev. Lett. **54**, 1317 (1985).
[7]See, for example, I. Affleck, Phys. Rev. B **37**, 5186 (1988).
[8]P. W. Anderson, Phys. Rev. **86**, 694 (1952).
[9]S. Chakravarty, B. I. Halperin, and D. Nelson, Phys. Rev. Lett. **60**, 1057 (1988); Phys. Rev. B **39**, 2344 (1989).
[10]R. R. P. Singh, Phys. Rev. B **39**, 9760 (1989); R. R. P. Singh and D. A. Huse, *ibid.* **40**, 7247 (1989).
[11]A. Auerbach and D. P. Arovas, Phys. Rev. Lett. **61**, 617 (1988); D. P. Arovas and A. Auerbach, Phys. Rev. B **38**, 316 (1988).
[12]D. Huse and V. Elser, Phys. Rev. Lett. **60**, 2531 (1988).
[13]M. Takahashi, Phys. Rev. B **40**, 2409 (1989).
[14]J. Oitmaa and D. D. Betts, Can. J. Phys. **56**, 897 (1978); J. E. Hirsch and S. Tang (unpublished).
[15]J. D. Roger and A. P. Young, Phys. Rev. B **37**, 5978 (1988); M. Gross, E. Sanchez-Velasco, and E. Siggia, *ibid.* **39**, 2484 (1989); T. Barnes and A. S. Swanson, *ibid.* **37**, 9405 (1988).
[16]S. Miyashita, J. Phys. Soc. Jpn. **57**, 1934 (1988); Y. Okabe and M. Kikuchi, *ibid.* **57**, 4351 (1988).
[17]E. Manousakis and R. Salvador, Phys. Rev. Lett. **60**, 840 (1988); Phys. Rev. B **39**, 575 (1989). Their correlation lengths are close to ours for $T \geq 0.5J$.
[18]D. H. Lee, J. D. Joannopoulos, and J. W. Negele, Phys. Rev. B **30**, 1599 (1984); G. Gomez-Santos, J. D. Joannopoulos, and J. W. Negele, *ibid.* **39**, 4435 (1989).
[19]H.-Q. Ding and M. S. Makivić, Phys. Rev. Lett. **64**, 1449 (1990).
[20]M. Suzuki, Prog. Theor. Phys. **56**, 1457 (1976); J. Stat. Phys. **43**, 883 (1986).
[21]J. J. Cullen and D. P. Landau, Phys. Rev. B **27**, 297 (1983).
[22]F. T. Arecchi, E. Courtens, R. Gilmore, and H. Thomas, Phys. Rev. A **6**, 2211 (1972).
[23]M. Marcu, in *Quantum Monte Carlo Methods in Equilibrium and Non-Equilibrium Systems,* edited by M. Suzuki (Springer, Berlin, 1987), p. 64.
[24]D. C. Mattis, in *The Theory of Magnetism* (Harper & Row, New York, 1965), Chap. 6.
[25]E. Loh, D. J. Scalapino, and P. M. Grant, Phys. Rev. B **31**, 4712 (1985).
[26]For a review, see G. C. Fox, **1**, 63 (1989).
[27]H.-Q. Ding and M. S. Makivic, Caltech Report No. C3P-845, 1990 (unpublished).
[28]H.-Q. Ding, Caltech Report No. C3P-629, 1989 (unpublished).
[29]R. M. Fye, Phys. Rev. B **33**, 6271 (1986).
[30]J. E. Hirsch, D. J. Scalapino, R. L. Sugar, and R. Blankenbecler, Phys. Rev. B **26**, 5033 (1982).
[31]G. S. Rushbrooke, G. A. Baker, Jr., and P. J. Wood, in *Phase Transitions and Critical Phenomena,* edited by C. Domb and M. S. Green (Academic, New York, 1974), Vol. 3, Chap. 5.
[32]A. Wiesler, Phys. Lett. **89A**, 359 (1982).
[33]S. H. Shenker and J. Tobochnik, Phys. Rev. B **22**, 4462 (1980).
[34]D. J. Amit, in *Field Theory, the Renormalization Group, and Critical Phenomena* (World Scientific, Singapore, 1984).
[35]R. R. P. Singh, P. A. Fleury, K. B. Lyons, and P. E. Sulewski, Phys. Rev. Lett. **62**, 2736 (1989).
[36]H.-Q. Ding and M. S. Makivić, Phys. Rev. B **42**, 6827 (1990).
[37]J. W. Negele and H. Orland, in *Quantum Many-Particle Systems* (Addison-Wesley, New York 1988).